



PNNL-24025

Prepared for the U.S. Department of Energy
under Contract DE-AC05-76RL01830

Mitigation and Prediction of Spallation of Oxide Scales on Ferritic Stainless Steel

Yeong-Shyung Chou, Elizabeth Stephens, Zhijie Xu, Wei Xu, Brian Koepfel,
and Jeff Stevenson

Pacific Northwest National Laboratory, Richland, WA

February 4, 2015



Pacific Northwest
NATIONAL LABORATORY

*Proudly Operated by **Battelle** Since 1965*

DISCLAIMER

This report was prepared as an account of work sponsored by an agency of the United States Government. Neither the United States Government nor any agency thereof, nor Battelle Memorial Institute, nor any of their employees, makes **any warranty, express or implied, or assumes any legal liability or responsibility for the accuracy, completeness, or usefulness of any information, apparatus, product, or process disclosed, or represents that its use would not infringe privately owned rights.** Reference herein to any specific commercial product, process, or service by trade name, trademark, manufacturer, or otherwise does not necessarily constitute or imply its endorsement, recommendation, or favoring by the United States Government or any agency thereof, or Battelle Memorial Institute. The views and opinions of authors expressed herein do not necessarily state or reflect those of the United States Government or any agency thereof.

PACIFIC NORTHWEST NATIONAL LABORATORY

operated by

BATTELLE

for the

UNITED STATES DEPARTMENT OF ENERGY

under Contract DE-AC05-76RL01830

Printed in the United States of America

Available to DOE and DOE contractors from the
Office of Scientific and Technical Information,
P.O. Box 62, Oak Ridge, TN 37831-0062;
ph: (865) 576-8401
fax: (865) 576-5728
email: reports@adonis.osti.gov

Available to the public from the National Technical Information Service,
U.S. Department of Commerce, 5285 Port Royal Rd., Springfield, VA 22161
ph: (800) 553-6847
fax: (703) 605-6900
email: orders@ntis.fedworld.gov
online ordering: <http://www.ntis.gov/ordering.htm>



This document was printed on recycled paper.

(9/2003)

Table of Contents

Executive Summary	2
Introduction	3
Surface Modification Approaches	4
Results of Long-term Oxidation Tests	4
Results of Long-term Stack Fixture Tests	5
Interfacial Indentation Experiments	5
Oxide Scale Spallation Model	7
Results of Interconnect Lifetime Sensitivity Analysis	8
Results of Interconnect Surface Modification Analysis	8
Conclusions	9
Acknowledgments	9
References	10
Tables	11
Figures	14
Appendix	21

Executive Summary

This report, which supplements and updates a previous interim report (PNNL-22191), summarizes results from experimental and modeling studies performed by researchers at Pacific Northwest National Laboratory on behalf of the Solid-State Energy Conversion Alliance (SECA) Core Technology Program. The results indicate that application of physical surface modifications, such as surface blasting, prior to application of protective surface coatings can substantially increase oxide scale spallation resistance during long-term exposure to elevated temperatures (e.g., 800-850°C). To better understand and predict the benefits of surface modification, an integrated modeling framework was developed and applied to the obtained experimental results.

Introduction

In recent years, progress in materials and fabrication techniques have allowed for a reduction in SOFC operating temperatures to a range in which commonly used oxidation-resistant alloys, such as ferritic stainless steels, can be considered as replacement materials for the traditional ceramic interconnect materials used in high temperature SOFC stacks. One candidate steel, which offers appropriate CTE, good oxidation resistance, an electrically conductive oxide scale, and relatively low cost, is AISI 441.¹ AISI 441 is prepared via conventional melt metallurgy and is therefore less expensive than candidate steels that utilize vacuum processing to reduce the Si content to very low levels. Additions of Nb and Ti to the AISI 441 tie up residual Si in Laves phase at grain boundaries, eliminating the need for expensive processing. To reduce Cr volatility and improve scale adhesion and oxidation resistance, protective coatings, such as Ce-modified (Mn,Co)₃O₄ (Ce-MC) spinel, have been developed for application to the cathode side of the interconnect.²⁻⁶ Long-term testing of AISI 441 coupons coated with Ce-MC spinel has indicated stable, low area-specific resistance (ASR) for over 25,000 hours at 800°C in air. However, it was also observed that thermal cycling of spinel-coated coupons after long-term oxidation (e.g., ≥4,000 hours at 800°C) can result in spallation of the oxide scale (and the spinel coating above it) from the underlying steel substrate. The interfacial strength between the oxide scale and the substrate is crucial to the reliability and durability of the metallic interconnect in SOFC operating environments, as scale spallation could lead to increased Cr volatility and a substantial increase in electrical resistance.

To further investigate this issue, a study was initiated in order to determine whether surface treatments applied to AISI 441 prior to application of a spinel coating could result in improved oxidation/spallation resistance. Long-term oxidation tests were performed on spinel-coated steel coupons, which led to a down-selection to a preferred surface treatment (surface blasting). Subsequently, a long-term validation test of surface-blasted, spinel-coated AISI 441 was performed under realistic SOFC stack conditions using the Solid-state Energy Conversion Alliance (SECA) Core Technology Program stack test fixture. In parallel, an integrated experimental/analytical methodology for quantifying the interfacial strength between the oxide scale and metallic interconnect materials was developed, thereby establishing a modeling tool that is able to predict the life of interconnect candidate materials under typical SOFC operating conditions. This integrated approach can also be used to quantify the effects of different surface finishes, coating/oxide layer thicknesses, and different coating materials such that an optimized coating thickness and surface condition for interconnect candidates can be developed to satisfy SECA life requirements.

Surface Modification Approaches

A variety of physical surface modifications to AISI 441 were investigated to assess their potential for mitigating spallation issues. ATI Allegheny Ludlum provided sheet stock (0.02" thick) of AISI 441 with the following five surface conditions:

1. Mill reference (unmodified, except for hand polishing with #1200 grit paper)
2. De-siliconized (treated to sequester and remove silicon from the near surface of the sheet; an alternative to decreasing the Si content of the alloy)
3. Surface blasted (subjected to a grit/shot blast process to produce surface deformation)
4. Surface ground (subjected to surface abrasion to produce surface deformation)
5. Temper-rolled (subjected to a cold rolling process)

Coupons of the surface-treated steel were coated with Ce-MC spinel and subjected to oxidation testing in stagnant air at 800°C and 850°C. At 2,000 hour intervals, the coupons were cooled down to room temperature and examined. In some instances, a coupon representing one or more of the surface treatments was removed from the study for SEM/EDS evaluation, while the remaining coupons were reheated for continued testing.

Results of Long-term Oxidation Tests

Results of the oxidation study are summarized in Tables I and II for coupons oxidized at 800 and 850°C, respectively. Each row of the table summarizes observations after the designated cumulative oxidation time. The "Macroscopic Spallation" columns indicate whether or not visual inspection revealed any spallation at the scale/steel interface on any of the coupons subjected to a given surface treatment. A green color indicates that none of the coupons exhibited spallation, while an "X" with a red background indicates that spallation was observed on at least one of the coupons. A "XX" with a red background indicates that, after the listed time, no unspalled coupons remained for the given surface condition. For example, after 10,000 hours, all of the mill reference coupons being tested at 800°C had exhibited visual spallation of the oxide (and accompanying coating) from the steel substrate. The "Microscopic De-bonding" columns apply to coupons removed from the study for cross-section SEM analysis; these columns indicate whether or not the cross-section SEM analysis revealed any localized or complete (i.e., along entire length of cross section) de-bonding at the scale/steel interface. A green color indicates that the coupon exhibited no de-bonding, while an "L" with a red background indicates that localized de-bonding was observed, and a "C" with a red background indicates that complete de-bonding was observed.

The results of the oxidation tests indicated that all of the surface treatments resulted in improved spallation resistance relative to the unmodified mill reference condition. Surface blasting produced the best results, as none of the spinel-coated, surface-blasted coupons exhibited either localized de-bonding or macroscopic spallation, despite the fact that the surface blasted coupons

tended to exhibit a higher scale growth rate than most of the other surface treatments (Figure 1). A representative low magnification cross-section SEM image of a coupon oxidized for 30,000 hours at 800°C, shown in Figure 2, reveals the roughened surface morphology created by the surface blasting process, which may be at least partly responsible for the improved spallation resistance.

Cross-section SEM/EDS analysis was also performed to evaluate compositional changes in the coating over time. As would be expected thermodynamically, diffusion of Cr and Fe into the coating from the underlying scale and alloy led to an increased concentration of both elements over time. As shown in Figure 3 and Table III, after 30,000 hours at 800°C the Cr concentration in the coating was ~7-10 at%. Although this is substantial, it is much lower than would be the case for an exposed chromia-based scale. Results of Cr volatility experiments on Cr-containing MnCo spinel (being performed by a partner institution) will be reported when they become available.

Results of Long-Term Stack Fixture Tests

Following up on the encouraging results observed with small surface-blasted coupons, two long-term tests were performed in PNNL's stack test fixture (Figure 4). These tests allowed the surface modification to be evaluated at a larger scale under conditions that resemble the operating conditions and environment of real-world SOFC stacks. Two tests were performed: one with an AISI 441 interconnect plate that was surface-blasted with #40 (coarse) grit, and one with a plate that was surface-blasted with #80 (fine) grit. Surface roughness measurements indicated that the #40 and #80 grits resulted in average surface roughness of 4.62 and 3.30 μm , respectively. (The roughness of the interconnect blasted with #80 grit was similar to that of the material originally provided by Allegheny Ludlum). Both interconnect plates were coated (via aerosol spray deposition) with Ce-MC spinel after the surface blasting was performed. Other stack test components included commercial anode-supported cells (5 cm x 5 cm) with LSM-based cathodes, LSM and NiO contact pastes, and de-vitrifying glass seals. The tests were performed in constant current mode at 800°C for ~6,000 hours, followed by 9 deep thermal cycles to assess the spallation resistance. While some degradation in cell performance was observed during the test, there was no indication that the degradation was related to instability of the coated interconnects. Upon completion of the tests, the cells were dis-assembled for post-test analysis. No evidence of coating or scale spallation was observed during visual inspection of the interconnect plates. Similarly, cross-section SEM analyses revealed no evidence of de-bonding at either the coating/scale or scale/steel interfaces (Figure 5).

Interfacial Indentation Experiments

Interfacial indentation testing has been reported as an alternative to characterize the adhesive properties for thermal spray coatings^{7,8}. A Vickers indenter is applied to a sample cross section to generate and propagate a crack along the interface between the coating and the substrate

materials. The indentation load and the length of the cracks generated at the interface are then measured from a series of tests. These values can then provide a quantitative measure of the apparent fracture toughness, or interfacial strength, of the “interface material” which represents the coating adhesion. Figure 6 shows a schematic of the interfacial indentation test.⁷ The induced crack is located in the plane of the interface and has a half-penny shape.⁸

This indentation methodology was applied to the surface-blasted (SB) and surface-ground (SG) spinel-coated AISI 441 specimens from the long-term oxidation studies at 800 and 850°C. Micro- and nano-indentation was performed on cross-sections of the SB and SG surface modified populations for which no coupons had exhibited spallation or delamination at the end of a given thermal cycle. Up to five different loads, $P = 0.2, 0.375, 0.8, 1.2$ and 1.8 N, were applied to each specimen with a minimum of three indents at each load. Note that the greater load ranges were not always feasible due to the indent size created. After indentation, the crack lengths, a , the local oxide thickness, and the half-diagonal of each indent were measured optically as illustrated in Figure 7. Three local thickness measurements were also performed and then averaged for each indentation. The crack lengths induced on each side of the indent were also averaged.

According to Chicot et al.,⁷ the relation between the crack length, a , and the applied load, P , is represented by a straight line for a given substrate and each coating thickness, e , on a logarithmic scale. These lines will converge and intersect at a critical load (P_c) and a critical crack length (a_c) that corresponds to the cracking ability of the interface for each surface condition. It must be noted that only results obtained where the generated crack remains in the interface plane are valid. Any deviation of the crack into the coating does not correspond to delamination of the interface. Hence in our data, results with cracks that violated this condition were discarded and only indentation results where the crack remained in the interface were analyzed. The natural log of the average crack length and load applied was determined for all valid indentation data and plotted.

Also according to the proposed theory, plotting of the relationship between the applied load and the indentation diagonal for indents that do not generate cracks will produce another straight line that passes through the critical point. These data points represent the relationship corresponding to the Vickers hardness (HV) of the interface. Therefore, a linear fit of these data points at the defined slope value of 0.5 from the standard Vickers hardness (HV) equation⁷ provides another line to identify the critical intersection point.

Due to the time intensive nature of obtaining sufficient indentation data, two adaptations of the Chico et al. methodology were made to improve the data analysis. First, local scale thickness for any given specimen did not vary enough to distinguish oxide scale thickness effects on the generated indentation crack size. Therefore, scale thickness was neglected and all cracked

indents for a given specimen were used to obtain the first fitted line. Second, the number of indents which did not crack for a given specimen was sometimes small. Therefore, indentation data with and without cracks were used to obtain the hardness line for a given specimen when necessary. This increased the fitting statistics without significantly changing the predicted interface hardness. The intersection of the indentation data linear fit and the apparent hardness then defines the critical parameters, P_c and a_c , as shown in Figure 8.

By combining the critical parameters for cracking, P_c and a_c , with the interface mechanical properties, the apparent interface fracture toughness (K_{in}) may be defined as

$$K_{in} = 0.015 \frac{P_c}{a_c^{3/2}} \left(\frac{E}{H} \right)_I^{1/2} \quad (1)$$

where P_c and a_c are the coordinates of the critical point. A (P_c, a_c) couple defines the visible interfacial crack initiation, where P_c is the applied load and a_c is the imprint diagonal of the indenter which equals to the crack length at this load level. The relationship $(E/H)_I$ is defined by

$$\left(\frac{E}{H} \right)_I^{1/2} = \frac{\left(\frac{E}{H} \right)_S^{1/2}}{1 + \left(\frac{H_S}{H_C} \right)^{1/2}} + \frac{\left(\frac{E}{H} \right)_C^{1/2}}{1 + \left(\frac{H_C}{H_S} \right)^{1/2}} \quad (2)$$

where E is the Young modulus, H is the hardness and the subscripts, S , C and I stand for the substrate, coating and interface, respectively.

Oxide Scale Spallation Model

Cooling of the SOFC stack from normal operating temperatures can result in delamination, buckling and spallation of the coating system due to mismatch of coefficients of thermal expansion (CTE) between the substrate, oxide scale, and coating layers. Therefore, a general modeling framework based on stress analysis and fracture mechanics was developed to predict the mechanical reliability and lifetime of the spinel-coated surface-modified specimens under isothermal cooling and thermal cycling.

The developed framework is shown in Figure 9, where the left half indicates the required physical testing and the right half indicates the fracture mechanics-based modeling. For physical testing, the interfacial fracture toughness K_{ic} and oxide growth kinetics are used as model inputs. Using metallographically prepared specimens from the long-term heat treatment experiments, the scale growth kinetics are determined by optical measurements of scale thicknesses and the fracture toughness is estimated by the interfacial indentation experiments described above.

For the fracture mechanics-based modeling, analytical solutions were formulated to evaluate the scale/substrate interfacial toughness Γ and the energy release rate G for buckling driven delamination under isothermal cooling, both of which are functions of the oxide thickness h . The interfacial fracture toughness K_{ic} from material testing is used to calculate the interfacial

toughness Γ . The critical oxide thickness h_c at which oxide scale fails can then be found from the failure criteria $G > \Gamma$. The predicted interconnect lifetime, i.e. the time required for oxide scale to grow to the thickness h_c , can then be inferred from the oxide growth kinetic curves. Due to uncertainties associated with the fracture toughness derived from the indentation, a systematic method to incorporate this uncertainty into the lifetime prediction was also developed. Complete details of the analytical model developed are provided in the Appendix.

Results of Interconnect Lifetime Sensitivity Analysis

Using the developed experimental/analytical methodology, a parametric study was performed on the effects of various design factors such as interfacial fracture toughness K_{ic} , thermal expansion coefficients, coating thickness, and compressive stress on the mean interconnect (IC) lifetime. Summary results of the sensitivity analysis are:

- IC lifetime increases significantly with increasing interface fracture toughness K_{ic} as expected.
- IC lifetime increases slightly with CTE of the coating layer, but decreases significantly with CTE of the substrate due to larger thermal mismatch stresses.
- IC lifetime increases almost linearly with coating layer thickness due to the additional elastic energy adsorbed by the coating layer during buckling.
- Compressive stress applied to the coating surface is beneficial to improve the interconnect lifetime, suggesting that IC regions in the active area subjected to stack preload will have a longer lifetime than unsupported regions.

Results of Interconnect Surface Modification Analysis

The methodology was then applied to the surface modified SS441 specimens from long-term testing at 800°C and 850°C. The predicted lifetimes and uncertainty of the various specimen conditions are shown in Figure 10. It is observed that SG specimens exhibited the highest individual strength/lifetime but also the widest range of predicted lifetime. Further analysis of the sample data indicated that no obvious trend in the predicted strength/lifetime was observed over the duration of the long term heat treatment. Also, no apparent difference between the 800°C and 850°C conditions was observed, and local oxide thickness variation at the indentation locations was not responsible for the observed strength differences. It was therefore concluded that all of the indentation data could be reasonably consolidated into SB and SG datasets.

The distributions of the interfacial stress intensity factor and critical oxide scale thickness for the SB and SG consolidated data are shown in Figure 11. The SG distribution contains two strong peaks suggesting that two different surface topologies may be present (i.e., regions of ‘good’ and ‘poor’ surface grinding). This is consistent with observations from microscopy which suggested that some regions of the SG material did not receive the same amount of grinding as others. Optimization of the SG process to eliminate the lower strength regions could result in a more uniform improvement similar to that observed in the SB material.

The predicted probability and cumulative distribution functions for both treatments are shown in Figure 12. The predicted results indicate that, if the specimen data is representative of the overall interconnect response, neither material would experience any failures through 25k hours at 800°C. The predicted failure rate of the unsupported interconnect would be ~10% at 30k hours and ~40% at 40k hours. Comparing to the long term heat treatment experiments, the model is conservative for the SB treatment as no failures were observed through 32k hours. The model is not conservative for the SG treatment. The cumulative distribution taken from the experimental SG results, where failures at 12k, 20k, and 22k hours were observed, is also shown in Figure 12b. This further supports the hypothesis that the SG application was undesirably not uniform, leading to some regions experiencing premature failure.

Conclusions

The main results from the long term heat treatment experiments and developed experimental/analytical lifetime methodology can be summarized as follows:

1. Physical surface modification of ferritic stainless steel prior to application of protective spinel coatings can significantly improve resistance to spallation at the oxide scale/steel substrate interface during long-term exposure to elevated temperatures (e.g., 800-850°C).
2. An integrated modeling framework combined with interfacial indentation experiments was established to predict the mean interconnect lifetime and its uncertainty.
3. For the specific surface modifications studied experimentally, the surface blast modification was found to be more uniform and superior to surface grinding. The predicted operating duration of an unsupported surface-modified interconnect is ~30k hours, at which point local buckling delamination may occur, possibly leading to degradation of interconnect performance. The model results are conservative relative to the experimental results, as no failures were observed through 32k hours.

In summary, a quantitative prediction of interconnect lifetime together with the associated uncertainty was implemented in a combined experimental/analytical framework to support SECA's material development and design efforts.

Acknowledgements

The work described in this report was funded by the Solid-state Energy Conversion Alliance Core Technology Program (US DOE-Fossil Energy). The authors wish to acknowledge helpful discussions with Briggs White and Shailesh Vora (NETL). The authors also thank Matt Bender of ATI Allegheny Ludlum for providing surface modified AISI 441 sheets.

References:

1. Z.G. Yang, G.G. Xia, C.M. Wang, Z. Nie, J.D. Templeton, J.W. Stevenson, and P. Singh, J. Power Sources, 183, 660 (2008).

2. Z.G. Yang, G.G. Xia, and J.W. Stevenson, *Electrochem. and Solid-State Letters*, 8, A168 (2005).
3. Z.G. Yang, G.G. Xia, X.H. Li, and J.W. Stevenson, *Int. J. of Hydrogen Energy*, 32, 3648 (2007).
4. Z.G. Yang, G.G. Xia, Z. Nie, J.D. Templeton, and J.W. Stevenson, *Electrochem. and Solid-State Letters*, 11, B140 (2008).
5. Z.G. Yang and J.W. Stevenson, "Durability of Metallic Interconnects and Protective Coatings," Chapter 35 in *Handbook of Fuel Cells: Advances in Electrocatalysis, Materials, Diagnostics and Durability*, W. Vielstich, H.A. Gasteiger, and H. Yokohawa, eds., p. 531, Wiley & Sons, West Sussex, UK (2009).
6. J.W. Stevenson, Z.G. Yang, G.G. Xia, Z. Nie, and J.D. Templeton, *J. Power Sources*, 231, 256 (2013).
7. D. Chicot, P. Demarecaux, and J. Lesage, *Thin Solid Films*, 283, 151 (1996).
8. G. Marot, P. Demarecaux, J. Lesage, A. Hadad, S. Siegmann, and M. Staia, *Surface & Coatings Technology*, 202, 4411 (2008).

Table I. Summary of results of 800°C oxidation study.

Time (h)	Mill Reference (1200 grit)		Temper Rolled		De-siliconized		Surface Grind		Surface Blast	
	Macroscopic Spallation	Microscopic De-bonding	Macroscopic Spallation	Microscopic De-bonding	Macroscopic Spallation	Microscopic De-bonding	Macroscopic Spallation	Microscopic De-bonding	Macroscopic Spallation	Microscopic De-bonding
2000										
4000	X									
6000	X			C	X					
8000	X			C						
10000	XX	XX		C				L		
12000	XX	XX					X	L		
14000	XX	XX				L				
16000	XX	XX								
18000	XX	XX								
20000	XX	XX				L	X	L		
22000	XX	XX		#		#	X	#		#
24000	XX	XX		#		#		#		#
26000	XX	XX		#		#		#		#
28000	XX	XX		#		#		#		#
30000	XX	XX				L		L		
32000	XX	XX		#		#		#		#

X - spallation on at least one coupon

XX - no unspalled coupons left in study

C - complete de-bonding of scale of SEM/EDS sample

L - localized de-bonding of scale of SEM/EDS sample

- coupon not removed for analysis due to limited number of coupons remaining in study

Table II. Summary of results of 850°C oxidation study.

Time (h)	Mill Reference (1200 grit)		Temper Rolled		De-siliconized		Surface Grind		Surface Blast	
	Macroscopic Spallation	Microscopic De-bonding	Macroscopic Spallation	Microscopic De-bonding	Macroscopic Spallation	Microscopic De-bonding	Macroscopic Spallation	Microscopic De-bonding	Macroscopic Spallation	Microscopic De-bonding
2000										
4000		L								
6000		C								
8000		C				C				
10000	X		X			C				
12000	X		X		X	C				#
14000	X		X		X	L				#
16000	XX	XX		#		#		#		#
18000	XX	XX		#		#		#		#
20000	XX	XX			XX	XX				
22000	XX	XX		#	XX	XX		#		#
24000	XX	XX		#	XX	XX		#		#
26000	XX	XX			XX	XX		L		

X - spallation on at least one coupon

XX - no unspalled coupons left in study

C - complete de-bonding of scale of SEM/EDS sample

L - localized de-bonding of scale of SEM/EDS sample

- coupon not removed for analysis due to limited number of coupons remaining in study

Table III. EDS results for the regions shown in Figure 3 (atomic %).

Spectrum	O	Al	Si	Ti	V	Cr	Mn	Fe	Co	Ce
Spectrum 1	58.74			0.69		6.63	16.81	3.90	13.06	0.18
Spectrum 2	58.09			0.67		7.50	16.58	3.89	13.13	0.14
Spectrum 3	59.02			0.61		8.15	15.60	3.70	12.83	0.09
Spectrum 4	57.98		0.42	0.56		9.57	15.12	3.52	12.66	0.17
Spectrum 5	58.03		0.26	0.54		11.55	13.91	3.23	12.34	0.13
Spectrum 6	58.43			0.68		9.09	15.29	3.65	12.66	0.21
Spectrum 7	57.01		0.31	0.76		8.37	16.28	3.83	12.99	0.45
Spectrum 8	62.54			0.18		35.98	0.76	0.22	0.32	
Spectrum 9	62.05		0.26	0.23		36.45	0.60	0.24	0.17	
Spectrum 10	61.80			0.33		37.00	0.58	0.28		
Spectrum 11	59.46		0.68	0.66	0.14	37.47	0.53	1.05		
Spectrum 12	5.44	0.45	1.00	0.77		18.07		74.27		
Spectrum 13		0.51	1.09	0.65		17.69		80.05		

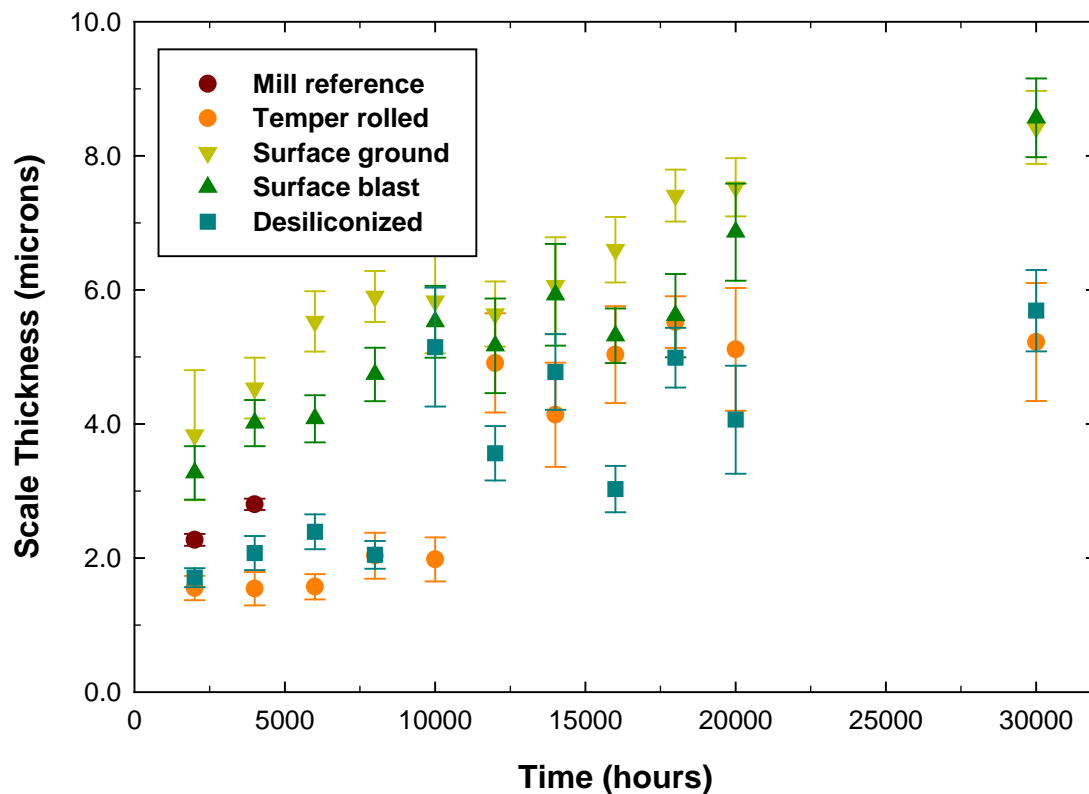


Figure 1. Average oxide scale thickness of spinel-coated AISI 441 with the indicated surface conditions as a function of time. Samples were oxidized in air at 800°C.

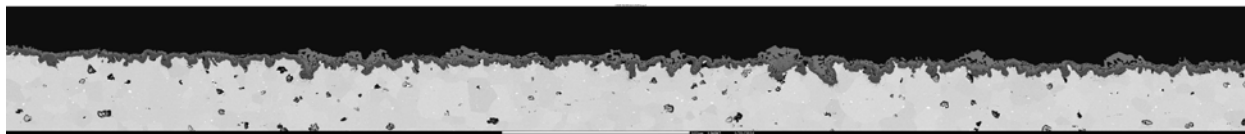


Figure 2. SEM micrograph of spinel-coated AISI 441 after 30,000 hours of oxidation in air at 800°C. Deep thermal cycles were performed every 2,000 hours. The chromia-based scale (dark gray) is visible between the spinel coating (top layer, light gray) and steel substrate (bottom).

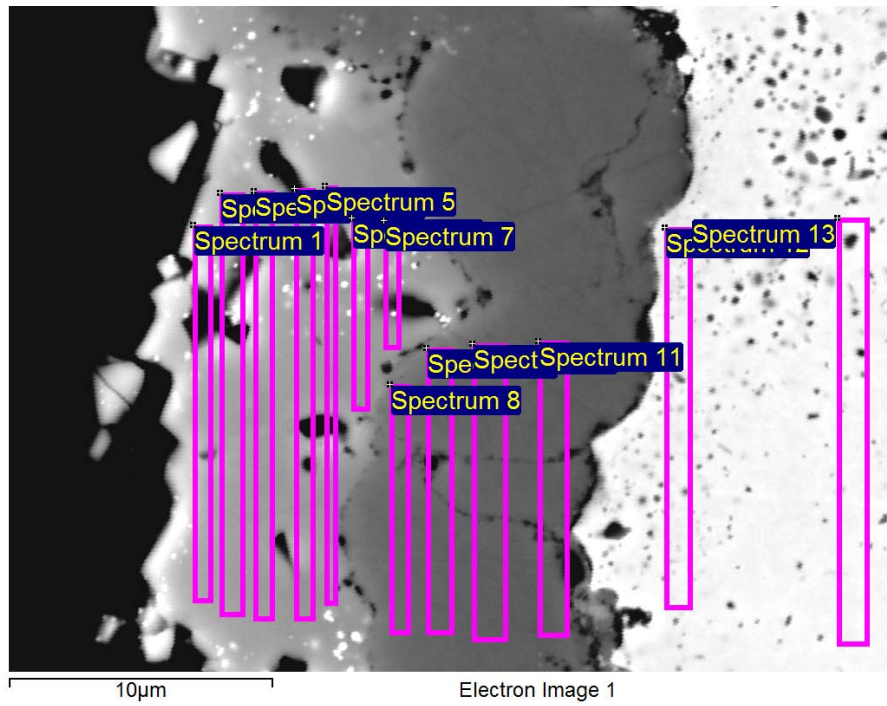


Figure 3. SEM/EDS analysis of surface blasted, spinel-coated AISI 441 after 30,000 hours of oxidation in air at 800°C. EDS results for the indicated regions are listed in Table III.

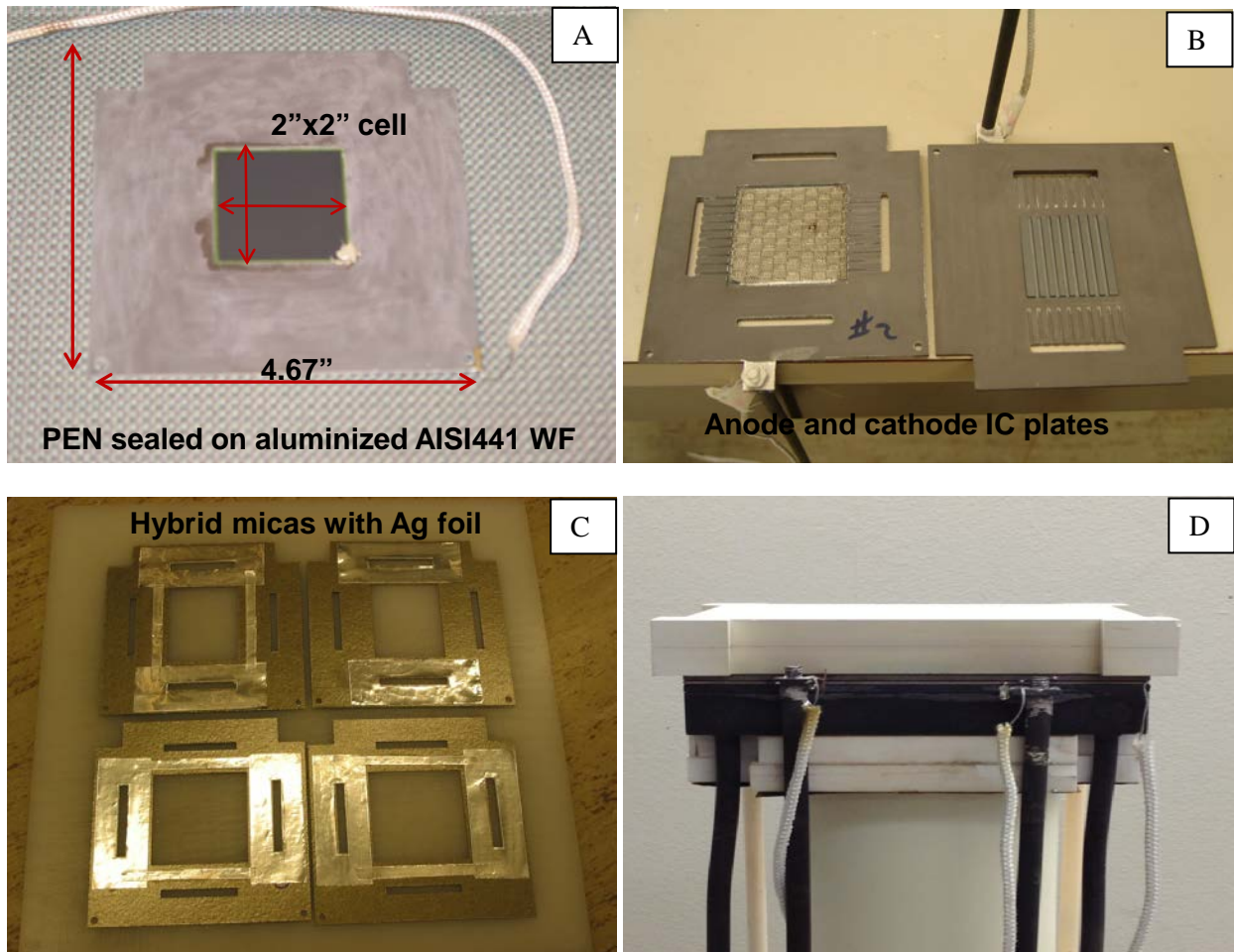
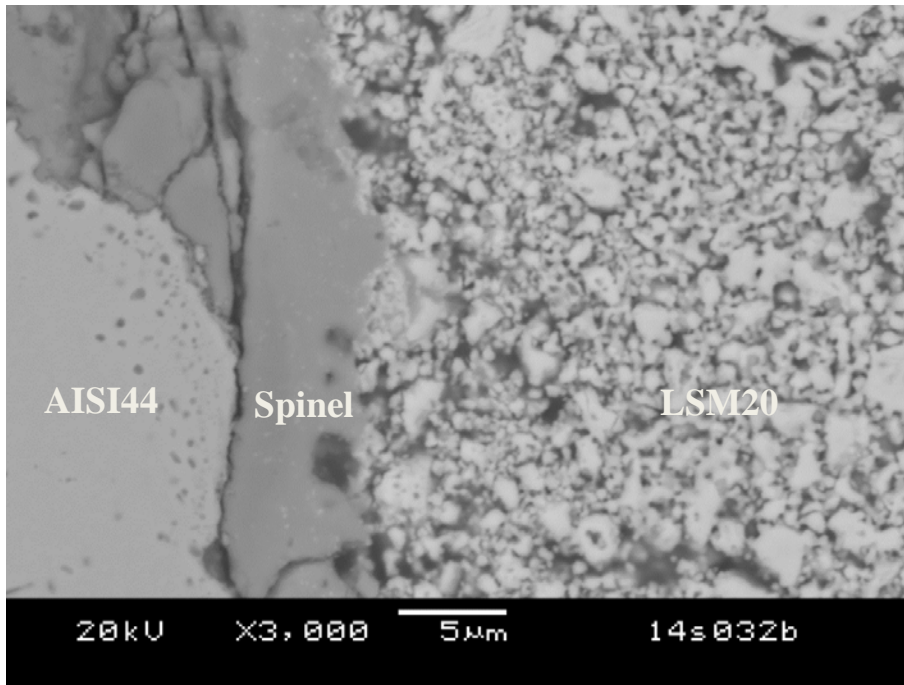
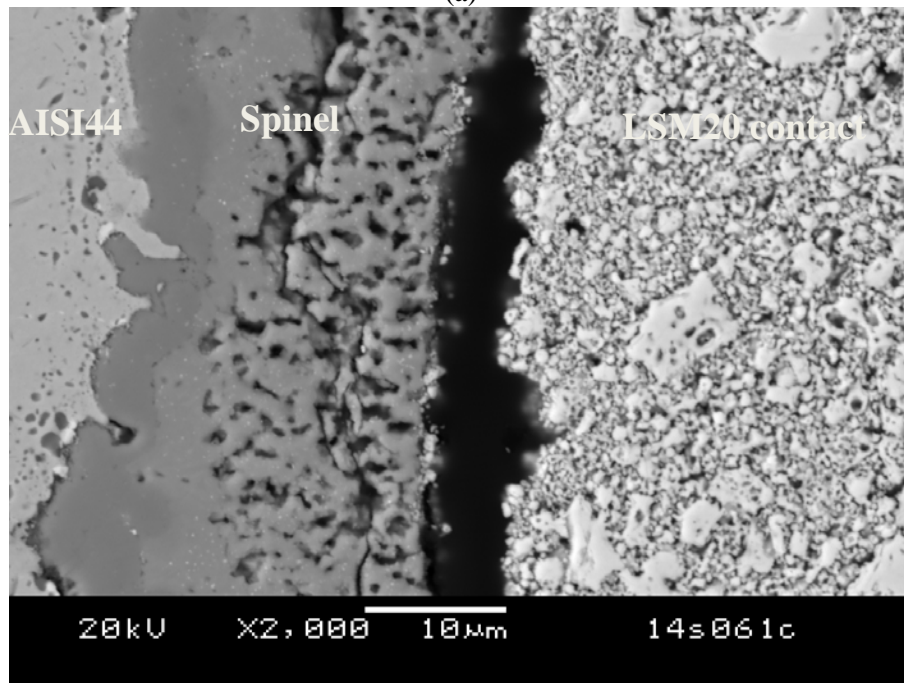


Figure 4. Photographs showing the cell assembly for single cell stack fixture test: (A) cell sealed onto aluminized AISI 441 cell frame plate; (B) anode-side interconnect plate with welded Ni mesh, and cathode-side spinel-coated, aluminized interconnect plate; (C) hybrid mica perimeter seals; (D) assembled view with top porous alumina and bottom Inconel 600 load block and heat-exchangers.



(a)



(b)

Figure 5. Representative microstructures of the spinel-coated AISI 441 after long-term stability and thermal cycling test at 800°C: a) surface blasted with coarse grit; b) surface blasted with fine grit.

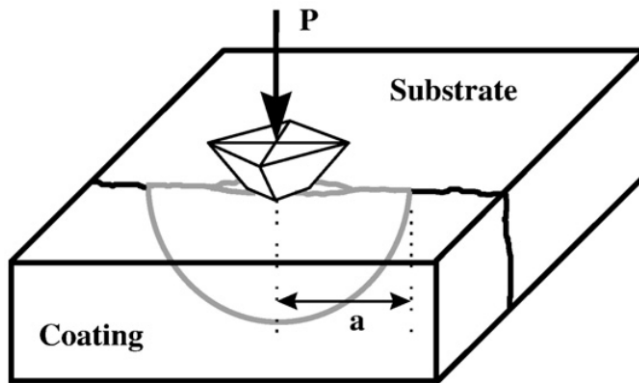


Figure 6. A schematic of the Vickers indentation test for interfacial analysis.

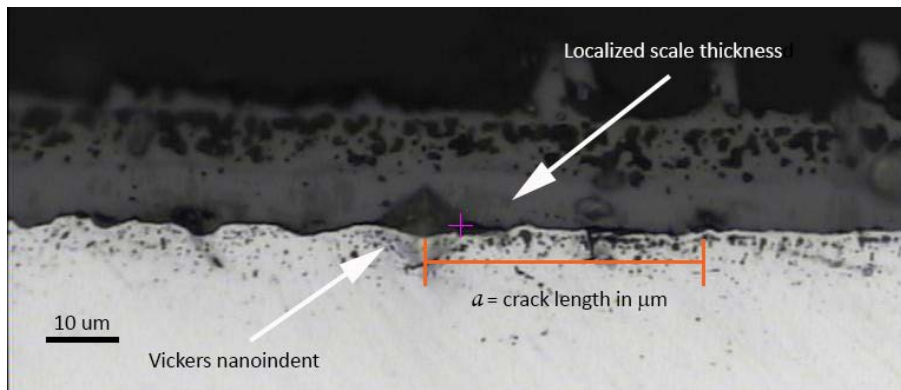


Figure 7. Representative image of a surface ground specimen indented at 375 mN indicating crack length measurement.

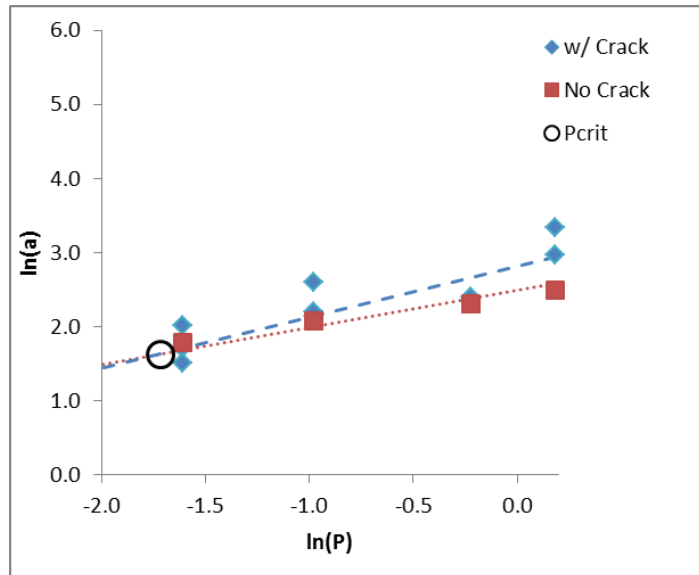


Figure 8. Representation of the cracking ability of an SB specimen exposed to 20,000h at 850°C where the critical load, P_c , and critical crack length, a_c , were determined.

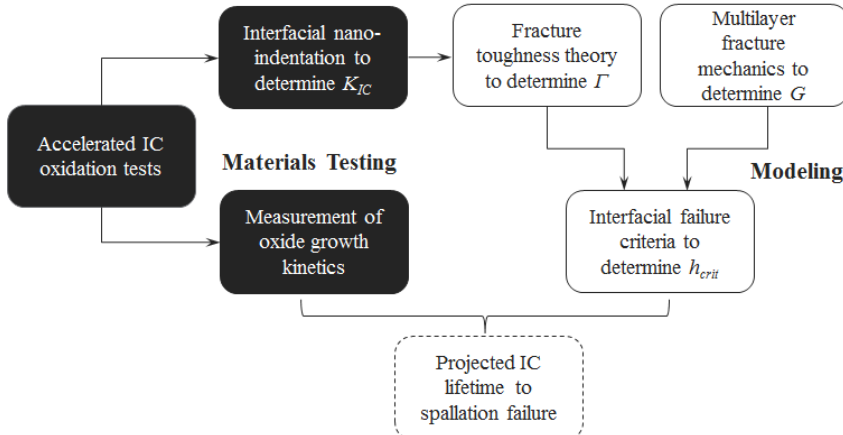


Figure 9. Flow chart for IC life prediction methodology.

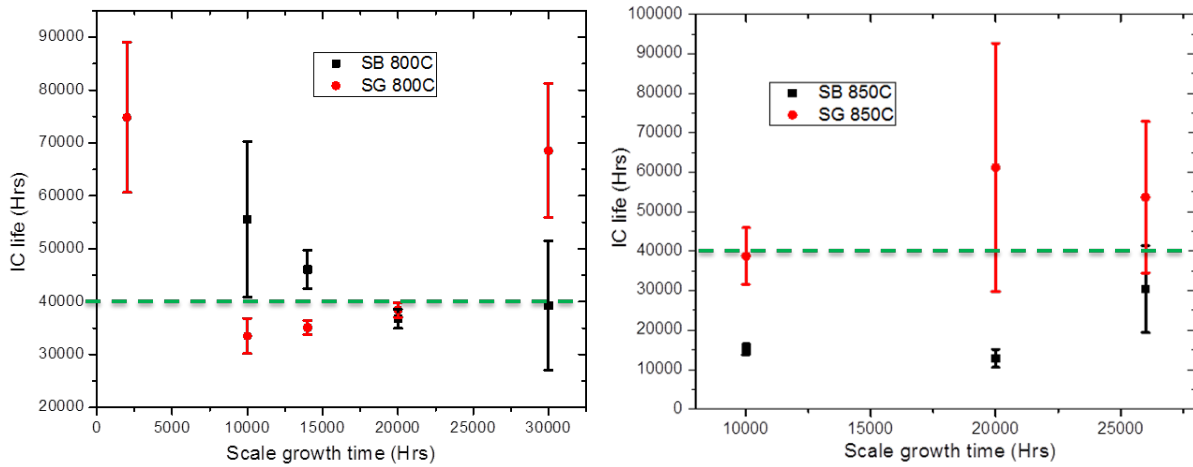


Figure 10. Measured mean lifetimes for SB and SG surface modified SS441 specimens at a) 800C and b) 850C.

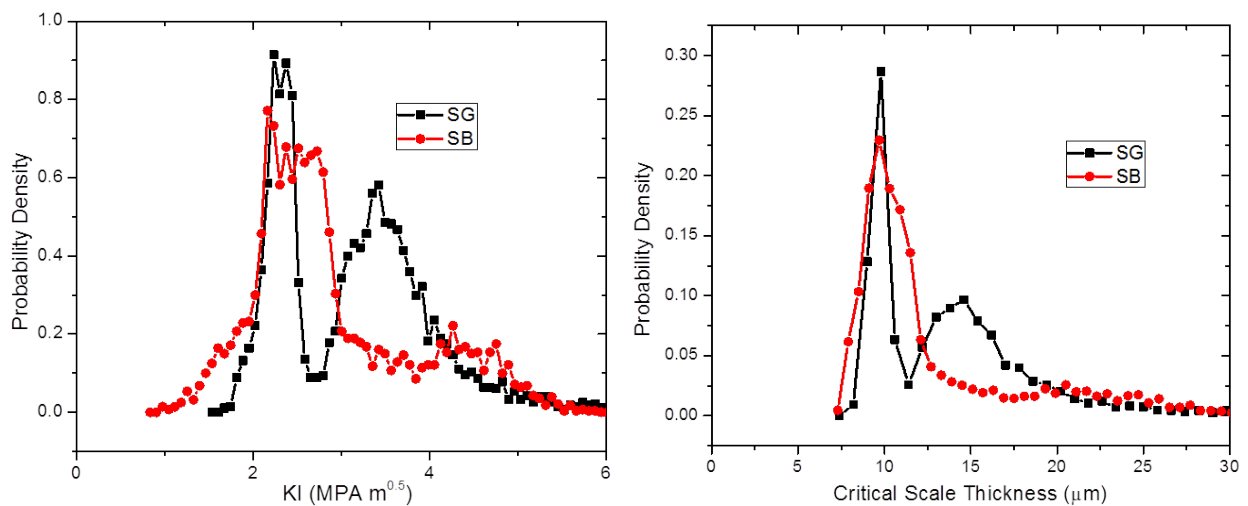


Figure 11. Expected distributions of the a) interfacial stress intensity factor and b) critical oxide scale thickness for the SB and SG specimen based on experimental measurements.

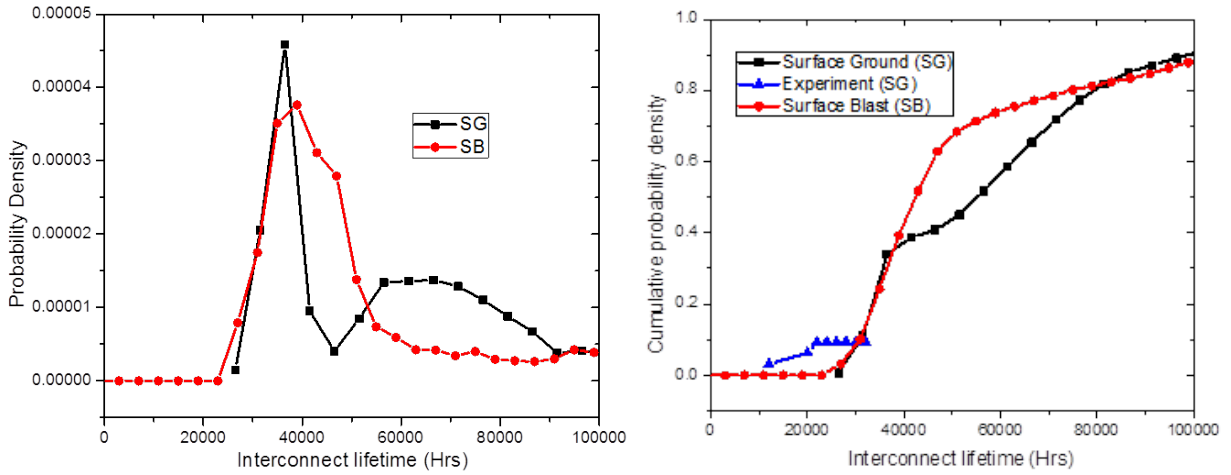


Figure 12. Expected a) probability density function and b) cumulative distribution function for the SB and SG modified SS441 specimens.

Appendix

Integrated modeling framework

A schematic plot of a coated metallic interconnect (IC) with multilayers of dissimilar materials is illustrated in Figure 1. The elastic response of each layer subjected to a uniform temperature decrease ΔT during isothermal cooling can then be given as

$$\sigma_s = E_s \frac{E_1 h_1 (\alpha_s - \alpha_1) + E_2 h_2 (\alpha_s - \alpha_2)}{E_1 h_1 + E_2 h_2 + E_s h_s} \Delta T \quad (1)$$

$$\sigma_1 = E_1 \frac{E_2 h_2 (\alpha_1 - \alpha_2) + E_s h_s (\alpha_1 - \alpha_s)}{E_1 h_1 + E_2 h_2 + E_s h_s} \Delta T \quad (2)$$

$$\sigma_2 = E_2 \frac{E_s h_s (\alpha_2 - \alpha_s) + E_1 h_1 (\alpha_2 - \alpha_1)}{E_1 h_1 + E_2 h_2 + E_s h_s} \Delta T \quad (3)$$

where E is the elastic modulus, α denotes the coefficient of thermal expansion (CTE), h represents the thickness, and the subscripts s , 1, and 2 correspond to the substrate, oxide scale, and coating respectively.

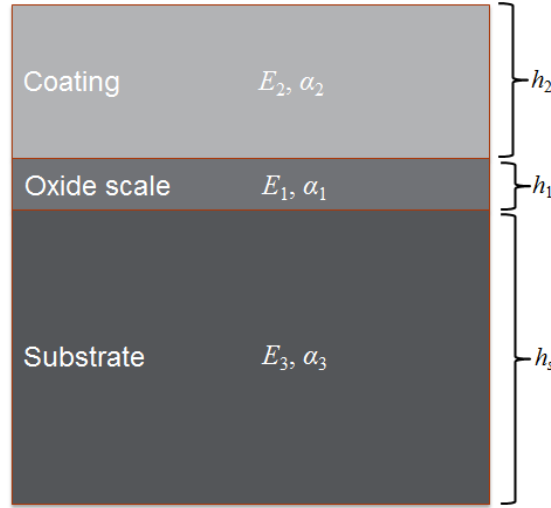


Figure 1. Multilayered structure of a coated IC.

As interfacial failures of ICs generally stem from these accumulated CTE mismatch-induced thermal stresses, two failure modes, namely buckling driven blistering and edge delamination, are commonly observed, where the first is primarily driven by the compressive stress in the adhesive thin film and the latter is caused by CTE mismatch induced shear stress.¹ Since significant shear traction is found to be limited to the near-corner regions of the films, the buckling driven blistering is considered to be of major concern to the interfacial cracking,² for which the failure criteria is typically defined as

$$G \geq \Gamma \quad (4)$$

with G denoting the energy release rate that represents the released elastic energy per unit of newly created fracture surface area and Γ is a critical value of G .

Accounting for the buckling driven blistering of a multi-layer structure in which the substrate is significantly thicker than the adhesive thin film, an analytical plane-strain solution for the energy release rate G is³

$$G = \frac{(1-\nu_f^2)h_f\sigma_c^2}{2E_f} \left(1 - \frac{\sigma_c}{\sigma_f}\right) \left(1 + 3\frac{\sigma_c}{\sigma_f}\right) \quad (5)$$

Here ν_f is the Poisson's ratio and σ_c is the critical buckling stress given by

$$\sigma_c = \frac{\pi^2 E_f}{12(1-\nu_f^2)} \left(\frac{h_f}{b}\right)^2 \quad (6)$$

with b denoting the size of the intrinsic interfacial blister. It should be noted that Eq. (6) is only valid when $\sigma_f \geq \sigma_c$.

One can then extend the present formulation to include the additional effects of the coating layer on the overall fracture resistance following a similar energy approach.

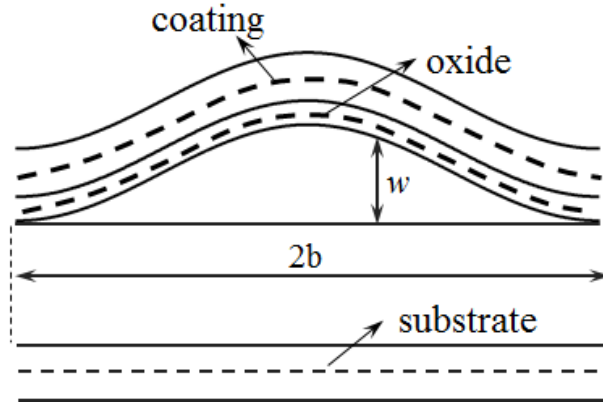


Figure 2. Auxiliary buckling problem of a coated IC.

The auxiliary buckling problem of a coated metallic IC illustrated in Figure 2 shows an oxide scale and a coating film clamped along their edges with no separation/slip between the coating and scale. The thermally induced compressive stress in the oxide scale brings a change to the multilayer curvature for which the corresponding deformation is given by the nonlinear Von Karman plate theory as:⁴

$$\Delta = \frac{1}{2} \int_{-b}^b w'^2 dy = 2b \frac{1-\nu_1^2}{E_1} (\sigma_1 - \sigma_c) \quad (7)$$

Therefore, the in-plane strain due to such buckled shape deformation imposed onto the coating layer can then be expressed as

$$\varepsilon^s = \frac{\Delta}{2b} = \frac{1-\nu_1^2}{E_1} (\sigma_1 - \sigma_c) \quad (8)$$

If we further denote the thermal strain within the coating layer to be ε_2 , the elastic energy build-up in the coating layer caused by the oxide scale buckling is given as

$$S_{\varepsilon} = \frac{E_2}{1-\nu_2^2} [(\varepsilon^* + \varepsilon_2)^2 - \varepsilon_2^2] b h_2 \quad (9)$$

where $\varepsilon_2 = \frac{1-\nu_2^2}{E_2} \sigma_2$ with E_2 , ν_2 , and h_2 corresponding to the elastic modulus, Poisson's ratio, and thickness of the coating layer.

As a result, the energy available for the buckling driven blistering fracture process is accordingly reduced. If we now re-define the original bi-layer energy release rate shown in Eq.(5) as G_0 , the updated G for the three-layer coated IC yields

$$G = G_0 - \frac{1}{2} \frac{\partial S_{\varepsilon}}{\partial b} = \frac{1-\nu_2^2}{2E_2} (\sigma_1 - \sigma_c) [h_1 (\sigma_1 + 3\sigma_c) - \frac{E_2}{E_1} \frac{1-\nu_2^2}{1-\nu_1^2} h_2 (\sigma_1 - \sigma_c) - 2\sigma_2 h_2] \quad (10)$$

It should be noted that here the critical buckling stress σ_c is currently assumed to be independent of the coating layer as h_1 is usually far greater than h_2 although expressions of enhanced accuracy for σ_c can be obtained through further finite element analyses.

Defined as the critical G for the crack tip to advance, Γ has been found to be strongly dependent on the mode mixity that can be expressed as:⁵

$$\Gamma = \Gamma_1 (1 + \tan^2[(1 - \lambda)\psi]) \quad (11)$$

where $\Gamma_1 = \frac{1-\nu_2^2}{E_1} K_{IC}^2$ is related to the apparent interfacial fracture toughness measurement K_{IC} which can be determined from indentation test, and ψ is the phase angle describing the mixity of the fracture failure Mode I and II for which a functional form can be written as

$$\tan \psi = \frac{4 + \sqrt{3}\xi \tan \omega}{-4 \tan \omega + \sqrt{3}\xi} \quad (12)$$

Here $\xi = \sqrt{\frac{4}{3} \left(\frac{\sigma}{\sigma_c} - 1 \right)}$ and $\omega = \omega(D_a)$ is a function of the Dundurs mismatch parameter D_a . When similar elastic properties of the substrate and the film materials hold, $D_a=0$ can be approximated and $\omega=52.07^\circ$. λ reflects the mode-dependency of Γ and has been reported to be able to capture trends for the available experimental data sets with a value between 0.1 and 0.3.³

Given material properties (Table 1) of the other IC components, i.e. substrate and coating, as well as the SOFC operating conditions, a typical plot of G and Γ with oxide scale thickness h_1 can be presented in Figure 3. Since it appears that due to the mode mixity Γ decreases with h_1 while G approaches to the opposite, a critical scale thickness h_c for interfacial cracking failure can then be identified based on Eq. (4). Furthermore, by correlating the predicted h_c to the growth kinetics measurement of the oxide scale (shown in Figure 4), the IC lifetime to spallation failure can be finally estimated.

In the present study, the lifetime of a metallic SOFC IC of Cr-Fe-based alloy coated with a spinel protective layer has been evaluated, for which the material properties and geometric parameters are listed in Table 1 and two different surface modifications, surface ground (SG) and surface blast (SB), have been applied.

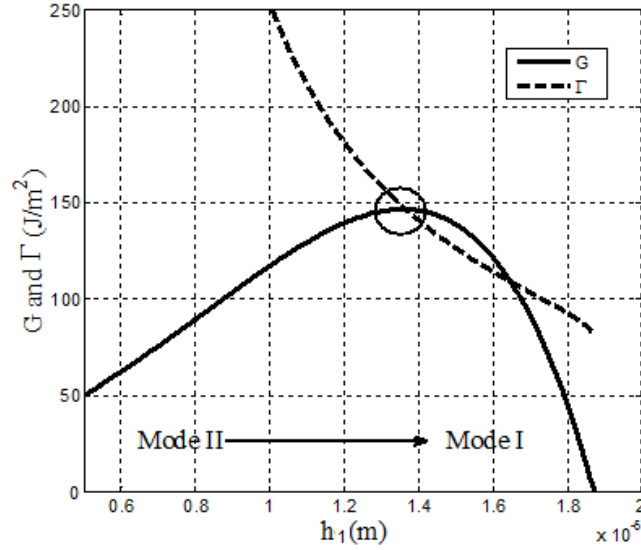


Figure 3. Typical variation of G and Γ with h_1 .

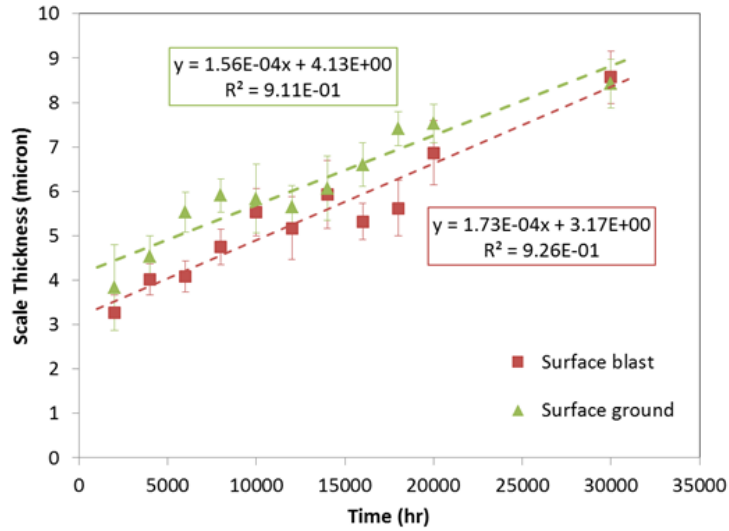


Figure 4. Measurements of oxidation kinetics for coated SB and SG IC specimens at 800°C.

With the K_{IC} measurements given by the interfacial nano-indentation tests for SB and SG samples to be $2.5 \text{ MPa}\cdot\text{m}^{0.5}$ and $2.2 \text{ MPa}\cdot\text{m}^{0.5}$, the critical thickness h_{cr} can be identified as $10.5 \text{ }\mu\text{m}$ and $9.5 \text{ }\mu\text{m}$ respectively.

Since the measurements of oxidation kinetics for the two types of samples shown in Figure 4 yield the linear scale thickness growth functions as

$$h_1 = \begin{cases} 1.56e^{-4}t + 4.13 & \text{coated SB sample} \\ 1.73e^{-4}t + 3.17 & \text{coated SG sample} \end{cases} \quad (15)$$

where t is in the duration time in hours, their expected lifetime can be determined accordingly as

$$t_L = \begin{cases} 44783 & \text{coated SB sample} \\ 31173 & \text{coated SG sample} \end{cases} \quad (16)$$

Table 1 Material properties and geometric parameters used in the present IC lifetime estimation

Symbol	Physical meaning	Value	Unit
E_s	Young's modulus (substrate)	200	GPa
E_1	Young's modulus (oxide)	250	GPa
E_2	Young's modulus (coating)	124.7	GPa
ν_s	Poisson's ratio (substrate)	0.3	Dimensionless
ν_1	Poisson's ratio (oxide)	0.27	Dimensionless
ν_2	Poisson's ratio (coating)	0.36	Dimensionless
α_s	Coefficient of thermal expansion (substrate)	12.4×10^{-6}	1/K
α_1	Coefficient of thermal expansion (oxide)	5.7×10^{-6}	1/K
α_2	Coefficient of thermal expansion (coating)	11.5×10^{-6}	1/K
h_s	Thickness (substrate)	5×10^{-4}	m
h_3	Thickness (coating)	1.5×10^{-5}	m
ΔT	Temperature change during stack cooling	775	K

Effects of interfacial fracture toughness K_{IC} and coefficients of thermal expansion

The interfacial fracture toughness K_{IC} is considered to be of major significance to the mechanical reliability of the multilayered structure.

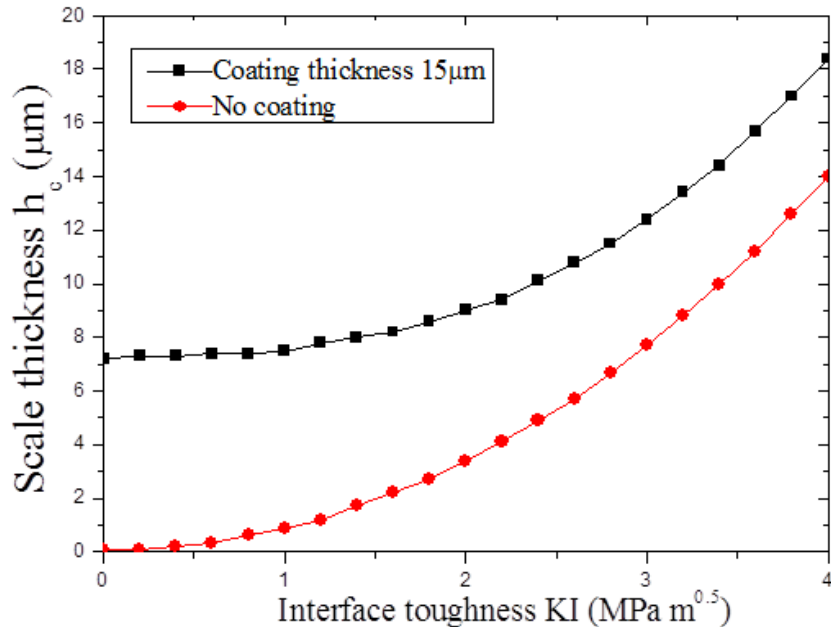


Figure 5. Effects of interfacial fracture toughness K_{IC} .

Figure 5 shows the variation of h_c with K_{IC} for both coated and uncoated specimens, where higher K_{IC} has been generally observed to yield greater h_c because of the enhanced interface strength and material fracture resistance. As the protective coating layer is able to provide additional confinement to tolerate the buckling instability induced by the oxide scale, it benefits the mechanical integrity and leads to significantly larger critical thickness of oxide scale. Because the spallation induced IC failure originates from the accumulated thermal stresses during operational stack cooling, the CTEs of individual IC design components, i.e. the substrate alloy and the coating layer, are critical factors in raw material selection.

As shown in Figure 6, the predictions of the critical scale thickness h_c against the thermal expansion coefficients of the substrate (α_s) and the coating (α_2) appear to follow opposite trends. It has been found that for both SG and SB IC specimens the critical scale thickness h_c (or interconnect life) is proportionally increasing with α_2 and significantly decreasing with α_s , the substrate coefficient of thermal expansion.

The uncertainty associated with the lifetime prediction.

Although the measurement accuracy can be improved with advanced evaluation techniques, statistical observational errors are still usually inevitable. Quantification of the influence of such input uncertainties on the outcome projections then becomes important to evaluate the predictive confidence level. The uncertainty in interconnect life prediction introduced from the indentation data can be quantitatively determined. The proposed methodology is able to predict both the mean value and the associated uncertainty for critical scale thickness and interconnect life time. The current modeling methodology takes the fracture toughness values measured from indentation test as the input to predict the lifetime of

interconnect. Uncertainties associated with the calculation of the interfacial roughness from the indentation data can be important to the prediction of interconnect lifetime. A systematic method to incorporate this uncertainty into the lifetime prediction was developed. In this section, indentation results from 10,000 h 800°C specimens are used as an example to demonstrate the method (Figure 7).

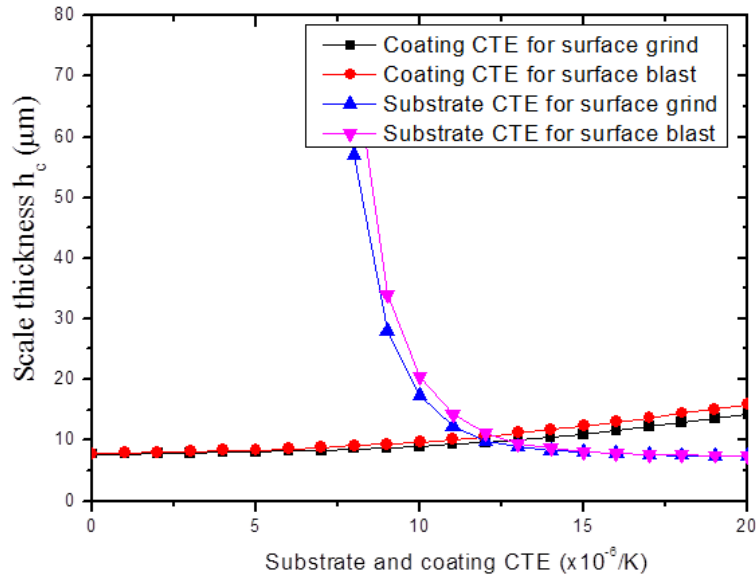


Figure 6. Effects of thermal expansion coefficient.

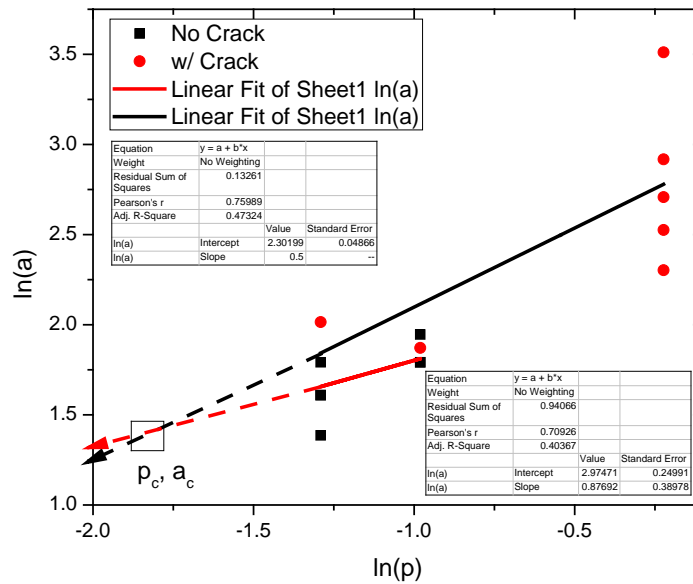


Figure 7. Determination of a_c and p_c from indentation data.

First, we have classified the indentation data into the data set “No Crack” and the data set “w/ Crack”. Two lines are obtained by linear fitting the “No Crack” and the “w/ Crack” data. The critical indentation load p_c and crack length a_c can be obtained as the interception of the two lines. The mean and the variance of the interception and slope of each line can be obtained from the linear regression analysis that was shown in the following table.

	Intercept (mean)	Intercept (std)	Slope (mean)	Slope (std)
No Crack	2.30199	0.04866	0.5	0
W/ Crack	2.97471	0.2499	0.87692	0.38978

Next, from the mean and the standard deviation of slope and intercept of two lines, a Monte Carlo simulation can be run to generate replicas. For each replica, the critical indentation load p_c and the crack length a_c can be computed. The fracture toughness value can be further calculated for each set of p_c and a_c from Eq. (13). The mean and standard deviation of p_c , a_c , and KI for 10,000 hrs at 800C are summarized in the next table. The probability distributions of p_c , a_c , and KI are also shown in Figure 8.

$$K_{in} = 0.015 \frac{P_c}{a_c^{3/2}} \left(\frac{E}{H} \right)_I^{1/2} \quad (13)$$

	ln(p_c)	ln(a_c)	KI
mean	-1.7826	1.4106	2.9937
std	0.6753	0.3501	0.5121

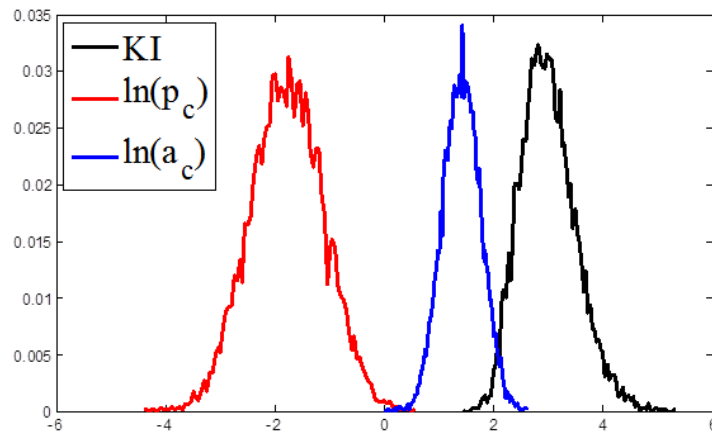
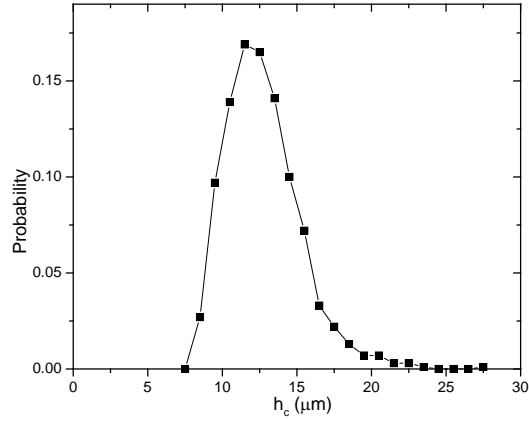


Figure 8. Probability distribution function of p_c , a_c and toughness KI.

Thirdly, the critical scale thickness h_c can be calculated for each fracture toughness value K_I using the interconnect lifetime model. For a given coating thickness and lateral stress, the calculated mean and standard deviation of h_c , and its probability distribution are shown in Figure 9 and the accompanying table.



	h_c (μm)
mean	12.76
std	2.51

Figure 9. Probability distribution of critical thickness h_c .

Finally, the interconnect lifetime mean, standard deviation and its probability distribution can be determined from the oxidation kinetic curves (shown in Figure 4) with computed critical scale thickness h_c . The oxidation kinetics measured from experiment was shown in Figure 4 for both surface blast (red symbol) and surface ground (green symbol). Therefore, the predicted interconnect lifetime and associated uncertainty can be estimated from the indentation data at 10,000hrs and 800C. The probability distribution and the cumulative distribution of interconnect lifetime were shown in the Figures 10 and 11. Up to this stage, we have demonstrated the methodology to predict the lifetime of interconnect using the indentation data with associated uncertainty of the prediction.

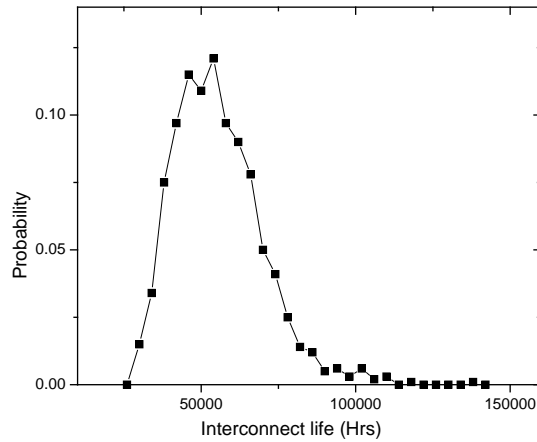


Figure 10. Probability distribution function of predicted interconnect life time.

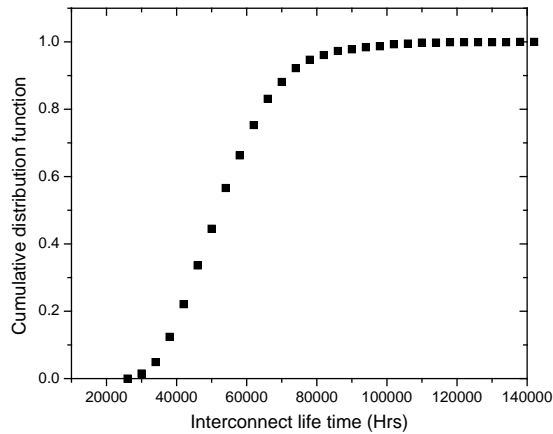


Figure 11. Cumulative distribution function of predicted interconnect life time.

Effect of coating thickness on the interconnect lifetime

Since it has been demonstrated that two beneficial effects on interconnect lifetime can be typically expected from the coating layer, i.e. slower oxide growth rate and improved mechanical stability, the overall effect of the coating layer on the critical scale thickness can be studied. The variations of critical scale thickness h_c with coating thickness h_2 for the two surface modifications, i.e. SG and SB, are shown in Figure 12. A monotonic proportional correlation between these two metrics has been observed, indicating that the thicker coating will generally strengthen the structure and increase the interconnect life time.

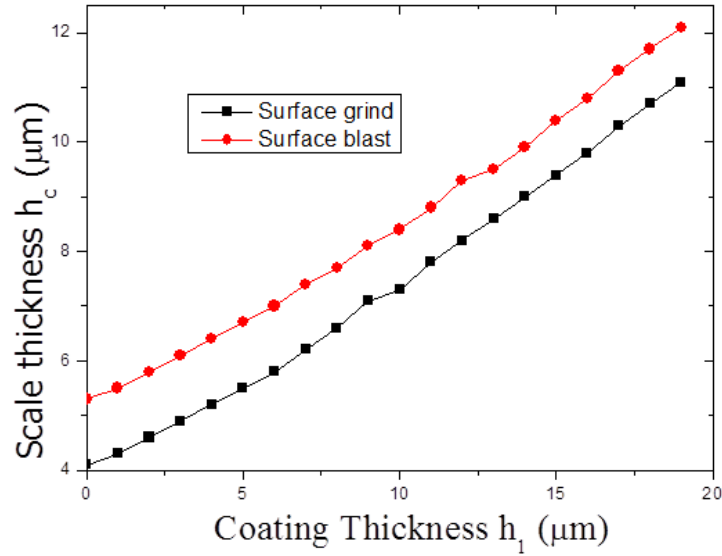


Figure 12. Effects of coating thickness h_3 .

Effect of lateral compressive stress on the oxide scale failure and interconnect lifetime

There could be lateral compressive stress applied on the coating for in-situ SOFC, as shown in Figure 13. In order to quantitatively consider the effect of this lateral compressive stress on the scale failure and interconnect lifetime, the energy release rate must be reformulated to include the terms due to the lateral compressive stress.

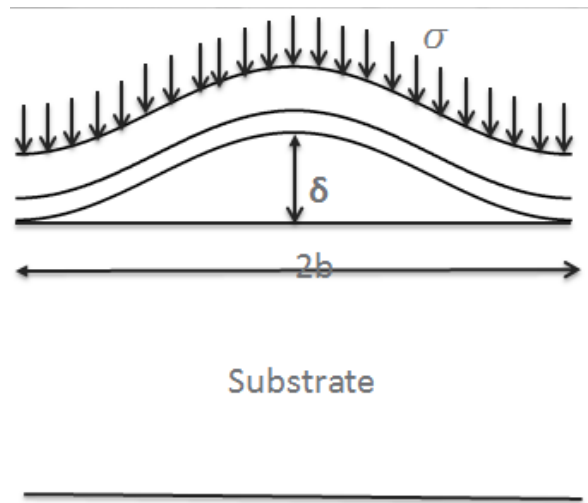


Figure 13. Illustration of lateral compressive stresses.

First, the work done by the lateral compressive stress, or equivalently the increase in the potential energy while buckling is

$$S_w = \int_{-b}^b \sigma_z w(x) dx \tag{14}$$

$$S_w = \sigma_z \delta b \quad (15)$$

where σ_z is the lateral compressive stress, w is the lateral deformation due to buckling, δ is the maximum deformation and b is the half size of the blister.

The energy release rate due to the lateral compressive stress can be written as:

$$\frac{\partial S_w}{\partial b} = \frac{\sigma_z \delta}{2} \quad (16)$$

The total energy release rate can be written as:

$$G = G^0 - \frac{1}{2} \frac{\partial S_e}{\partial b} - \frac{1}{2} \frac{\partial S_w}{\partial b} \quad (17)$$

with the first term representing the contribution from the scale, second term for the coating, and the third term from lateral stress, respectively. The modified interconnect model was implemented numerically. The modeling results are plotted in the next three figures.

Figure 14 shows the variation of the scale critical thickness with the coating thickness for different level of later compressive stresses. With increasing lateral compressive stress, the critical thickness (or equivalently the interconnect lifetime) is increasing. For a compressive stress of 0.2MPa, there is negligible increase in the critical thickness. The can also be shown in Figures 15 and 16, where critical thickness and lifetime were plotted against the lateral stress directly.

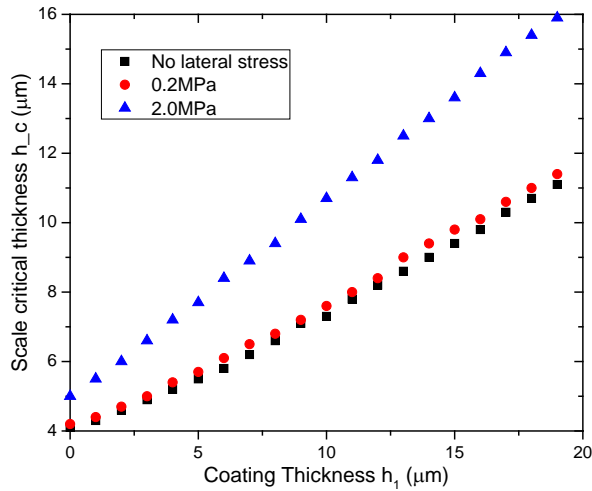


Figure 14. Variations of scale critical thickness with coating thickness for different later stresses.

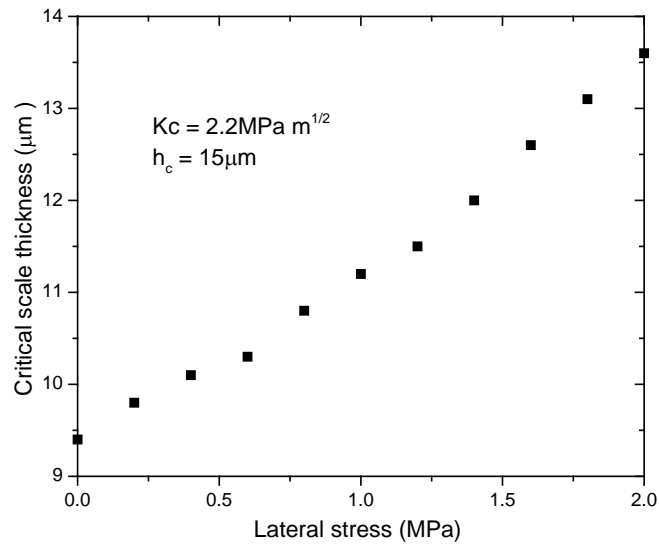


Figure 15. Variation of critical thickness h_c with lateral stress.

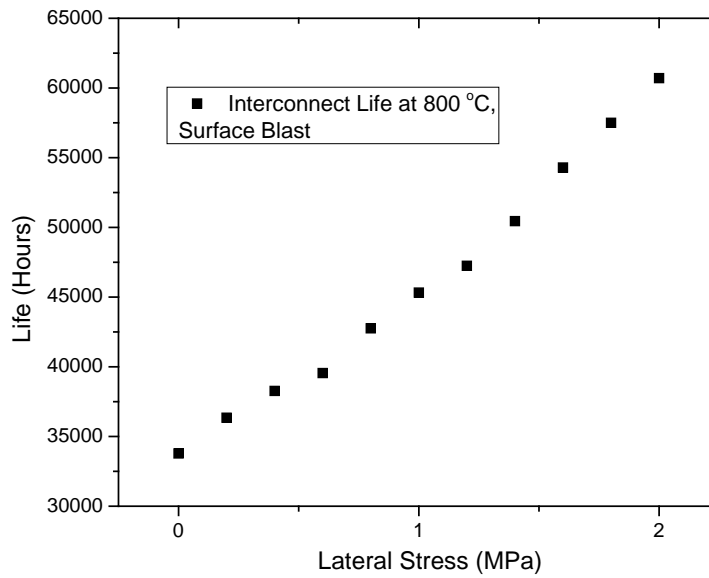


Figure 16. Variation of interconnect life time with lateral stress.

References

1. A.G. Evans and J.W. Hutchinson, *Acta Metallurgica et Materialia*, 43, 2507 (1995).
2. Yu, H. H., M.Y. He, and J.W. Hutchinson, *Acta Materialia*, 49, 93 (2001).

3. J.W. Hutchinson and Z. Suo, Advances in Applied Mechanics, 63 (1992).
4. H.H. Yu and J.W. Hutchinson, International Journal of Fracture, 113, 39 (2002).
5. J.W. Hutchinson, M.D. Thouless, and E.G. Liniger, Acta Metallurgica et Materialia, 40, 295 (1992).